PAPER

CrossMark
click for updates

Nanostructured biogel templated synthesis of Fe_3O_4 nanoparticles and its application for catalytic degradation of xylenol orange

Ya-Nan Chen, Tianqi Liu, Qin Zhang, Cong Shang and Huiliang Wang*

Easy preparation of well-dispersed inorganic nanoparticles is critical for their practical applications. By using jellyfish mesoglea, a biological hydrogel mainly composed of nanofibers, as a template, nanocomposite hydrogels with well-dispersed Fe_3O_4 nanoparticles are successfully synthesized through the co-precipitation method. Fe_3O_4 nanoparticles, mostly less than 20 nm, are uniformly formed and distributed on the nanofibers. With the increase of Fe^{2+}/Fe^{3+} concentration, more nanoparticles are formed and hence the size of the nanofibers increases, and only very less significant aggregation of Fe_3O_4 nanoparticles is observed at a high Fe^{2+}/Fe^{3+} concentration of 1 M. The JF/Fe_3O_4 nanocomposite hydrogels have very high Fe_3O_4 content, which can achieve about 79%. The nanocomposite hydrogels display nearly superparamagnetism, and show smaller saturation magnetizations (M_s) than that of bulk Fe_3O_4. Moreover, introduction of Fe_3O_4 nanoparticles increases the BET surface areas of the gels. The JF/Fe_3O_4 nanocomposite hydrogels exhibit high activity in catalyzing the oxidative degradation of xylenol orange and excellent reusability.

Introduction

Magnetic nanomaterials have widespread applications in drug release, hyperthermia, sensors, supercapacitors, adsorption, and catalysis.[1–6] The application of magnetic nanoparticles in catalysis has drawn rapidly growing attention due to their easy preparation, high catalytic efficiency, excellent reusability, and convenient separation from the reaction solutions by an external magnetic field.[7] Various kinds of magnetic nanoparticles, such as $MgCr_2O_4$, $Mn_xFe_{1-x}O$ and Fe_3O_4 nanoparticles, have been applied to catalyze the oxidative or photo degradation of pollutants in water, such as dyes, phenols, and bacteria.[6,8–10]

Fe_3O_4 nanoparticles are the most commonly used magnetic nanomaterials, and they are usually prepared through thermal decomposition, solvothermal reaction, co-precipitation and so on.[11–14] However, due to their inherent magnetic interactions and high surface energies, the aggregation of Fe_3O_4 nanoparticles is inevitable in many cases, which leads to their wide size distributions, small surface areas, and hence low catalytic efficiencies.[15,16] To prevent the aggregation of Fe_3O_4 nanoparticles, inorganic porous materials (*e.g.* alumina, silica and activated carbon) and macromolecular microspheres are commonly employed as the templates for the formation of Fe_3O_4 nanoparticles.[17–20] In addition, surfactants, capping

Beijing Key Laboratory of Energy Conversion and Storage Materials, College of Chemistry, Beijing Normal University, Beijing, 100875, P. R. China. E-mail: wanghl@bnu.edu.cn

agents, and chelating agents are also widely applied to increase the stability and activity.[21–23]

Hydrogels are three-dimensional polymeric networks containing a large portion of water. The polymeric networks can serve as ideal matrices for the formation of uniformly distributed Fe_3O_4 nanoparticles.[24] The incorporation of Fe_3O_4 nanoparticles into the hydrophilic gel network also facilitates the application of Fe_3O_4 nanoparticles in catalyzing the degradation of water pollutants.[6] Till now, several types of hydrogels with Fe_3O_4 nanoparticles have been reported. Fe_3O_4 nanoparticles can be introduced into the hydrogels before or after the gelation process[25–31] or simultaneously.[6,32]

However, most synthetic hydrogels are structurally inhomogeneous, and they generally show porous structures with continuous and dense pore walls (in the freeze-dried state), which impede the fast diffusion and exchange of masses between the hydrogels and the environment. The continuous and dense pore walls also lead to the low specific surface areas of the hydrogels, and hence severe aggregation of Fe_3O_4 nanoparticles is also observed in the hydrogels when the content of Fe_3O_4 nanoparticles is sufficiently high. Moreover, if the Fe_3O_4 nanoparticles are incorporated before or in the gelation process, then a large portion of them might be imbedded in the dense pore walls, and hence their performance is strongly impeded.

Hydrogels constructed of nanofibers and/or nanosheets should have very high specific surface areas, and hence provide more active sites for forming Fe_3O_4 nanoparticles. Unfortunately, the fabrication of nanostructured hydrogels remains

a challenge. Only very few such hydrogels have been reported, and the nanowires are usually made with template polymerization,[33,34] electrospinning,[35] and self-assembly.[36] Our group recently reported a novel directional freezing and γ-radiation initiated polymerization method for synthesizing hydrogels with aligned nanowires.[37] These methods are commonly very complex and time-consuming.

Thanks to their well-developed structures, biological hydrogels exhibit superior properties than synthetic hydrogels. Jellyfish mesoglea (hereafter shortened as JF gel) is a biological hydrogel mainly composed of nanofibers and nanosheets.[38,39] Macropores in micrometers and meshes in submicrons are constructed by the nanofibers and nanosheets. The unique nanostructured microstructure endows JF gel with good mechanical properties even at an extremely high water content of 97–99%.[40,41] Taking advantage of the JF gel's nanostructured porous structure, extremely high-content dendritic silver nanoparticles have been prepared by our group.[42] This novel biogel templated metal nanoparticle production method is very simple, cheap and high efficient, and it should be applicable for preparing other types of nanoparticles.

In this work, we used JF gel as a template to prepare Fe_3O_4 nanoparticles through co-precipitation. In addition, the application of the JF/Fe_3O_4 nanocomposite hydrogels in catalysis was demonstrated by catalyzing the oxidative degradation of xylenol orange. The Fe_3O_4 nanoparticles in the composite hydrogels exhibited high catalytic activity and excellent reusability.

Experimental

Materials

The edible jellyfish umbrella was purchased from seafood market, which was preserved with a mixture of table salt and alum. The inner part of the jellyfish mesoglea was cut from the jellyfish umbrella, and then it was firstly washed with tap-water and then washed with deionized water for 72 h to thoroughly remove the salts. Ferric chloride hexahydrate ($FeCl_3 \cdot 6H_2O$, analytical grade) and ferrous sulfate heptahydrate ($FeSO_4 \cdot 7H_2O$, 98%) were purchased from Shanghai Macklin Biochemical Co. Ltd. (Shanghai, China) and Alfa Aesar (Shanghai, China) chemicals Co. Ltd., respectively. Hydrochloric acid (HCl), ammonia water ($NH_3 \cdot H_2O$), nitric acid (HNO_3) and hydrogen peroxide (H_2O_2) were analytical grade from Beijing Chemical Works (Beijing, China), and xylenol orange tetrasodium salt ($C_{31}H_{28}N_2O_{13}SNa_4$, analytical grade) was from Tianjin Jinke Fine Chemical Institute (Tianjin, China). All chemicals were used without further purification.

Preparation of JF/Fe_3O_4 nanocomposite hydrogels

The swollen jellyfish mesoglea was cut into specimens with a size of 20 mm $\times$ 20 mm $\times$ 5 mm. The samples were dipped in a mixture of 25 mL $FeSO_4$ and 50 mL $FeCl_3$ (0.03 mol HCl added to prevent hydrolysis) with different original Fe^{2+} or Fe^{3+} concentrations (0.05, 0.1, 0.5 and 1.0 M) for 6 h (the Fe^{2+}/Fe^{3+} solution was changed after 3 h). Then the samples were put into a $NH_3 \cdot H_2O$ solution for 12 h to ensure the full reaction. The

dipping process and the reactions were carried out in a nitrogen atmosphere. Finally, the samples were thoroughly washed with deionized water to remove unreacted chemicals.

Characterization

X-ray diffraction patterns were recorded using a PANalytical-X' Pert PRO diffractometer (Cu radiation, $\lambda = 1.5418$ Å) running at 40 kV and 40 mA (PANalytical, Holland). X-ray photoelectron spectroscopy (XPS) was carried out on a LabRAM Aramis instrument (Horiba Jobin Yvon, France). Raman spectroscopy was performed on an ESCALAB 250Xi spectrometer (Thermofisher, UK) at room temperature.

ICP-AES analysis

The Fe_3O_4 nanoparticles in the composite hydrogels were reacted with concentrated HNO_3 to form water-soluble $Fe(NO_3)_3$, and then the diluted aqueous $Fe(NO_3)_3$ solutions were measured by inductively coupled plasma atomic emission spectroscopy (ICP-AES) on a SPECTRO ARCOS EOP instrument (SPECTRO Analytical Instruments GmbH, Germany). The contents of Fe_3O_4 in the solutions after the catalytic reactions were also measured with ICP-AES.

Superparamagnetism measurement

Magnetic properties of the products were investigated using a Superconducting Quantum Interference Device (SQUID, MPMS XL7, Quantum Design, USA) at room temperature.

Scanning electron microscopy (SEM) investigation

The samples were firstly frozen by rapidly plunging into liquid nitrogen for about 5 min, and then the frozen samples were freeze-dried in a LGJ-10C vacuum freeze dryer (Beijing Sihuan Scientific Instrument Factory, China) for about 24 h to remove water thoroughly. The freshly cracked surfaces of the freeze-dried samples were analyzed with a Hitachi S-4800 scanning electron microscope (Tokyo, Japan) with an accelerating voltage of 10 kV.

BET surface area analysis

The Brunauer–Emmett–Teller (BET) specific surface areas of the gel samples cracked into small lumps were evaluated on the basis of nitrogen adsorption isotherms using a Quantachrome NOVA 2000e sorption analyzer (Quantachrome, USA) at liquid nitrogen temperature.

Catalysis degradation of xylenol orange tetrasodium salt (XO)

For the catalysis degradation of XO, XO aqueous solution (1×10^{-4} M) was freshly prepared. In 10 mL XO solution, 10 mL H_2O_2 aqueous solution (30%) was added. One JF/Fe_3O_4 nanocomposite hydrogel sample, cut into eight pieces, was used for the catalysis degradation reaction carried out at ambient temperature under magnetic agitation. A Shimadzu UV-2450 spectrophotometer (Shimadzu, Japan) was employed to monitor the progress in a scanning range of 300–600 nm. With

a time gradient of every 5 min, a series of UV spectra were obtained.

Results and discussion

Preparation of JF/Fe$_3$O$_4$ nanocomposite hydrogels

JF/Fe$_3$O$_4$ nanocomposite hydrogels were prepared with the co-precipitation method. Firstly, JF gels (Fig. 1a) were dipped in the aqueous solutions containing both Fe^{2+} and Fe^{3+}, and in which the molar ratio of Fe^{2+} to Fe^{3+} is 1/2. After then, the JF gels with Fe^{2+} and Fe^{3+} (Fig. 1b) were soaked into a NH$_3\cdot$H$_2$O solution. The semitransparent JF gels became black in about 20 min (Fig. 1c), indicating the formation of Fe$_3$O$_4$ in the gels, and hence JF/Fe$_3$O$_4$ nanocomposite hydrogels were obtained.

Morphologies of Fe$_3$O$_4$ nanoparticles

The morphologies of an original JF gel and the JF/Fe$_3$O$_4$ nanocomposite hydrogels are displayed in Fig. 2. The original JF gel is mainly composed of smooth nanofibers with an average diameter of about 35 nm (Fig. 2a). When Fe$_3$O$_4$ is introduced into the JF gels, the surface of the nanofibers becomes rough and is covered with many nanoparticles (Fig. 2b–d). With the increase of Fe^{2+}/Fe^{3+} concentration, more nanoparticles are formed on the fibers and hence the size of the nanofibers increases. When the Fe^{2+}/Fe^{3+} concentration is increased to 1.0 M, adjacent fibers can even be merged to form larger fibers or sheets with a diameter or width up to several hundred nanometers due to the aggregation of the nanoparticles (Fig. 2d). The sizes of the nanoparticles are quite uniform, and they are mostly less than 20 nm, though very less significant aggregation of the nanoparticles is observed at a high Fe^{2+}/Fe^{3+} concentration. In short, the nanofibers in JF gel act as templates for the formation of nanoparticles.

Characterization of Fe$_3$O$_4$ nanoparticles

To confirm that the nanoparticles formed in the JF gels are Fe$_3$O$_4$, the dried composite hydrogels were firstly measured with XRD. As shown in Fig. 3, the (220) (311) (400) (422) (511) and (440) planes of Fe$_3$O$_4$ were observed at $2\theta = 30.20°$, $35.51°$,
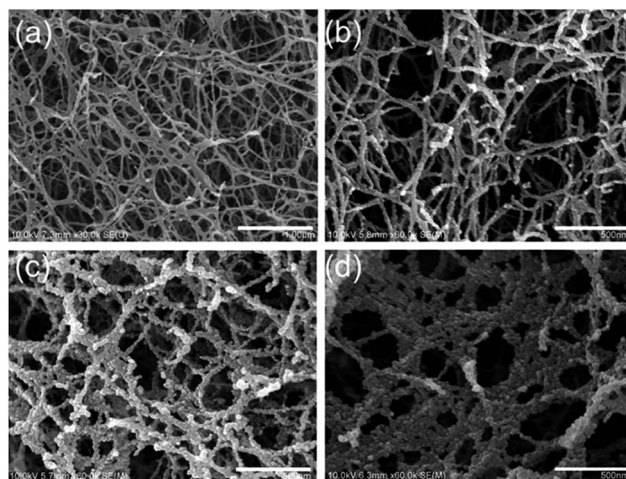

Fig. 2 SEM images of an original JF gel (a) and the JF/Fe$_3$O$_4$ nanocomposite hydrogels prepared at the Fe^{2+}/Fe^{3+} concentrations of 0.1 M (b), 0.5 M (c) and 1.0 M (d).

43.13°, 53.66°, 57.16° and 62.90°, respectively, which are consistent with JCPDS 19-629 (JCPDS: Joint Committee on Powder Diffraction Standards).[43]

It is well-known that the XRD patterns of Fe$_3$O$_4$ and γ-Fe$_2$O$_3$ are very similar, so the XRD pattern cannot provide enough evidence to rule out γ-Fe$_2$O$_3$.[44] Therefore, XPS and Raman spectra were both recorded to distinguish Fe$_3$O$_4$ from γ-Fe$_2$O$_3$. XPS is very sensitive to Fe^{2+} and Fe^{3+} ions. Fig. 4a shows the core-level XPS patterns of a JF/Fe$_3$O$_4$ nanocomposite hydrogel in the Fe 2p region. The peaks at binding energies of 710.3 and 724.1 eV are the characteristic doublet of Fe 2p$_{3/2}$ and Fe 2p$_{1/2}$ core-level spectra of Fe$_3$O$_4$, respectively. While the typical satellite peak at around 719.2 eV attributed to γ-Fe$_2$O$_3$ does not appear, excluding the presence of γ-Fe$_2$O$_3$ in the JF/Fe$_3$O$_4$ nanocomposite hydrogel.[45] Fig. 4b shows the Raman spectrum of the JF/Fe$_3$O$_4$ nanocomposite hydrogel. Four main peaks at the wavenumbers of 276, 390, 587 and 1288 cm^{-1} are almost identical to those reported for Fe$_3$O$_4$ powder, and no peaks at around 1430 and 1580 cm^{-1} attributed to γ-Fe$_2$O$_3$ are observed.[7] These characterizations substantially prove that the nanoparticles formed are Fe$_3$O$_4$.

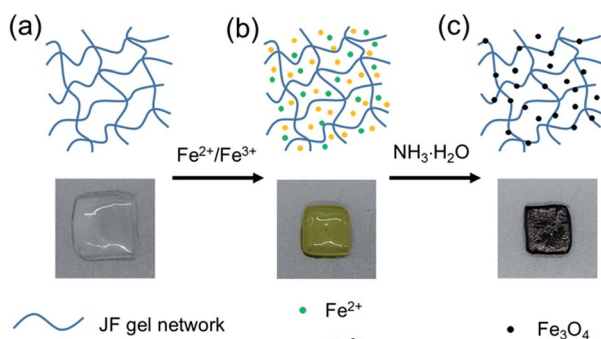Fig. 1 Schematic representation and photos showing the preparation of JF/Fe$_3$O$_4$ nanocomposite hydrogels. (a) An original JF gel, (b) the Fe^{2+}/Fe^{3+} loaded JF gel, and (c) the JF/Fe$_3$O$_4$ nanocomposite hydrogel.
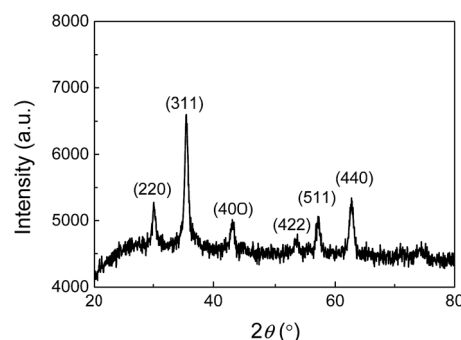
Fig. 3 X-ray diffraction pattern of the JF/Fe$_3$O$_4$ nanocomposite hydrogel prepared at a Fe^{2+}/Fe^{3+} concentration of 0.5 M.
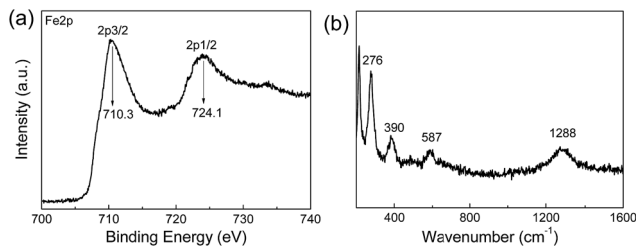
Fig. 4 Fe 2p core-level XPS spectrum (a) and Raman spectrum (b) of a JF/Fe$_3$O$_4$ nanocomposite hydrogel prepared at a Fe^{2+}/Fe^{3+} concentration of 0.5 M.

The contents of Fe$_3$O$_4$ nanoparticles in the composite gels measured with ICP-AES are shown in Fig. 5. The composite gels generally have very high Fe$_3$O$_4$ contents, from 32% at a very low Fe^{2+}/Fe^{3+} concentration of 0.05 M to the highest value of 79% at 1.0 M Fe^{2+}/Fe^{3+} concentration. The high Fe$_3$O$_4$ content in the composite gels is attributed to the extremely low solid content of JF gel (1–3 wt%) and the nanostructured macroporous structures that facilitate the migration of Fe^{2+}/Fe^{3+} ions and the formation of Fe$_3$O$_4$ nanoparticles. It is noticeable that the increase of Fe$_3$O$_4$ content with increasing Fe^{2+}/Fe^{3+} concentration becomes much slower at a higher concentration. The possible reason is the decrease of active sites on the nanofibers after the formation of some nanoparticles.

Magnetic properties

Magnetic hysteresis (M–H) loops of the JF/Fe$_3$O$_4$ nanocomposite hydrogel were measured by SQUID at 300 K. Fig. 6a shows the magnetization curve of the JF/Fe$_3$O$_4$ nanocomposite hydrogel prepared at a Fe^{2+}/Fe^{3+} concentration of 0.5 M. The coercivity (H_c) and remanence (B_r) observed in its enlargement tend to zero (see the inset), indicating that there is nearly not any remaining magnetization after removing external magnetic field. So it is reasonable to conclude that the Fe$_3$O$_4$ nanoparticles in the composite hydrogels exhibit superparamagnetic behavior.[46] The saturation magnetization (M_s) of the gel is about 32 emu g^{-1}, which is much smaller than that of bulk Fe$_3$O$_4$ (92 emu g^{-1}).[47] The small values of H_c, B_r and M_s could be all
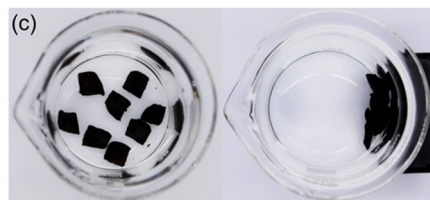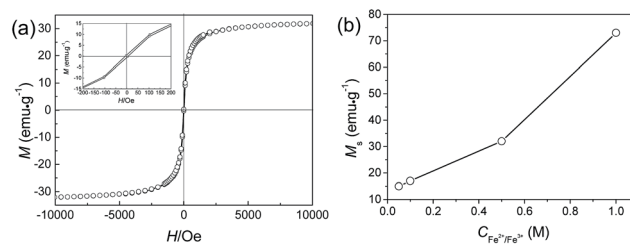

Fig. 6 (a) Magnetization curve of the JF/Fe$_3$O$_4$ nanocomposite hydrogel prepared at a Fe^{2+}/Fe^{3+} concentration of 0.5 M (inset: enlarged magnetization curve); (b) saturation magnetization (M_s) of JF/Fe$_3$O$_4$ nanocomposite hydrogels as a function of Fe^{2+}/Fe^{3+} concentration; (c) photos demonstrating the attraction of JF/Fe$_3$O$_4$ nanocomposite hydrogel specimens with a magnet.

attributed to the rather small size of the Fe$_3$O$_4$ nanoparticles prepared at a Fe^{2+}/Fe^{3+} concentration of 0.5 M.[7,48] Fig. 6b shows that M_s increases with the increase of Fe^{2+}/Fe^{3+} concentration, in consistent with the increase of Fe$_3$O$_4$ content and the aggregation of nanoparticles.[47]

The magnetic properties of the JF/Fe$_3$O$_4$ nanocomposite hydrogels endow them with easy collection and separation from solutions. As demonstrated in Fig. 6c, the hydrogel blocks placed in water in a beaker can be easily attracted with a magnet.

Brunauer–Emmett–Teller (BET) surface areas

The Brunauer–Emmett–Teller (BET) surface areas of the gels are shown in Fig. 7. The original JF gel has a relatively low surface area of 5.9 m^2 g^{-1}, possibly due to the low solid content and the smooth surface of the nanofibers. The surface areas of the JF/Fe$_3$O$_4$ nanocomposite hydrogels gradually increase with increasing Fe^{2+}/Fe^{3+} concentration, and the highest for the gel
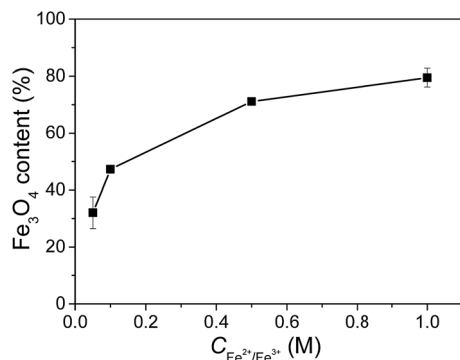

Fig. 5 Fe$_3$O$_4$ contents in the JF/Fe$_3$O$_4$ nanocomposite hydrogels prepared at different Fe^{2+}/Fe^{3+} concentrations.
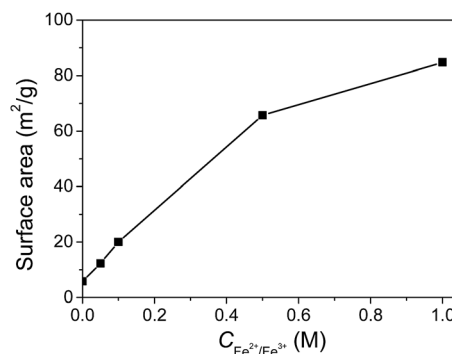
Fig. 7 Surface areas of the JF/Fe$_3$O$_4$ nanocomposite hydrogels as a function of Fe^{2+}/Fe^{3+} concentration.

prepared at a Fe^{2+}/Fe^{3+} concentration of 1.0 M is 85 m^2 g^{-1}. The increase of BET surface area should be ascribed to the introduction of Fe_3O_4 nanoparticles.

Catalytic properties

Using the strong oxidizer ˙OH produced through the decomposition of H_2O_2 catalyzed by Fe_3O_4 nanoparticles, organic pollutants can be degraded.[49] Here, we used the JF/Fe$_3$O$_4$ nanocomposite hydrogels as a heterogeneous catalyst to catalyze the degradation of xylenol orange tetrasodium salt (XO). The reaction process was monitored with UV-Vis spectroscopy, and the typical UV-Vis spectra are shown in Fig. 8a and b. In the absence of a JF/Fe$_3$O$_4$ nanocomposite hydrogel, the strong absorption peak at 434 nm attributed to XO keeps almost no change even after 45 min (Fig. 8a), suggesting that the degradation of XO does not occur, due to the difficulty in producing ˙OH. On the contrary, with the addition of a JF/Fe$_3$O$_4$ nanocomposite hydrogel, the absorbance at 434 nm gradually decreases with reaction time, and the peak vanishes in about 45 min (Fig. 8b). These results indicate that the JF/Fe$_3$O$_4$ nanocomposite hydrogel is very effective in catalyzing the decomposition of H_2O_2, which produces the strong oxidizer ˙OH for the degradation of XO.

The degradation of XO in the presence of H_2O_2 follows a pseudo first-order kinetics, and the apparent first-order rate constant k can be calculated through the following equation:

$$\ln(A/A_0) = \ln(C/C_0) = -kt$$

where $C_0(A_0)$ and $C(A)$ are the initial concentration (or absorbance) of XO and the concentration (or absorbance) at the reaction time t, respectively.

The $\ln(C/C_0)$–t curves of the reactions performed in the presence of a JF/Fe$_3$O$_4$ nanocomposite hydrogel for five successive cycles are shown in Fig. 8c. A linear $\ln(C/C_0)$–t relationship is found for all cycles. The corresponding slopes (k) of the fitted linear lines are 0.040, 0.038, 0.037, 0.037 and 0.035 min^{-1}, respectively (Fig. 8c), indicating the excellent recyclability of the JF/Fe$_3$O$_4$ nanocomposite hydrogel.

The k values of the JF/Fe$_3$O$_4$ nanocomposite hydrogels prepared at different Fe^{2+}/Fe^{3+} concentrations are shown in Fig. 8d. Obviously, the k value increases with Fe^{2+}/Fe^{3+} concentration. The apparent reason is the increase of Fe_3O_4 content in the hydrogels prepared with a higher Fe^{2+}/Fe^{3+} concentration. The k values obtained in this work are much higher than the values reported for palladium-modified TiO_2 nanoparticles (0.013 min^{-1})[50] and ZnS nanoparticles (0.0155 min^{-1}),[51] and they are comparable to the highest reported values for porous Fe_3O_4 nanospheres (0.056 min^{-1}).[7]

The Fe_3O_4 nanoparticles in the composite hydrogels are very stable in the catalysis process. We measured the contents of Fe_3O_4 in the reacted solutions with ICP-AES analysis and found that they are negligible. For example, in the XO and H_2O_2 solution after being catalyzed for 45 min by a JF/Fe$_3$O$_4$ nanocomposite hydrogel prepared at a Fe^{2+}/Fe^{3+} concentration of 1.0 M, there is only 7.37 μg Fe (or 30.53 μg Fe$_3$O$_4$), which is less than 0.04% of the amount of Fe_3O_4 nanoparticles in the nanocomposite hydrogel (*ca.* 80 mg).

Conclusions

In summary, we have successfully prepared well-dispersed Fe_3O_4 nanoparticles in the nanostructured jellyfish mesoglea which acts as a natural template for the formation of Fe_3O_4 nanoparticles. Thanks to the nanostructured macroporous structures of jellyfish mesoglea, Fe_3O_4 nanoparticles are formed and distributed on the nanofibers, avoiding their severe aggregation even at very high contents of Fe_3O_4. The introduction of Fe_3O_4 nanoparticles endows the hydrogels with good superparamagnetic properties and high BET surface areas. The JF/Fe$_3$O$_4$ nanocomposite hydrogels exhibit high catalytic activity as well as excellent reusability in the catalytic degradation of xylenol orange. The idea of using nanostructured biogels as templates to prepare inorganic nanoparticles can be further expanded to other biomaterials for producing other types of metal or metal oxide nanoparticles. The biogel/nanoparticle composite hydrogels may also find practical applications in many other fields.
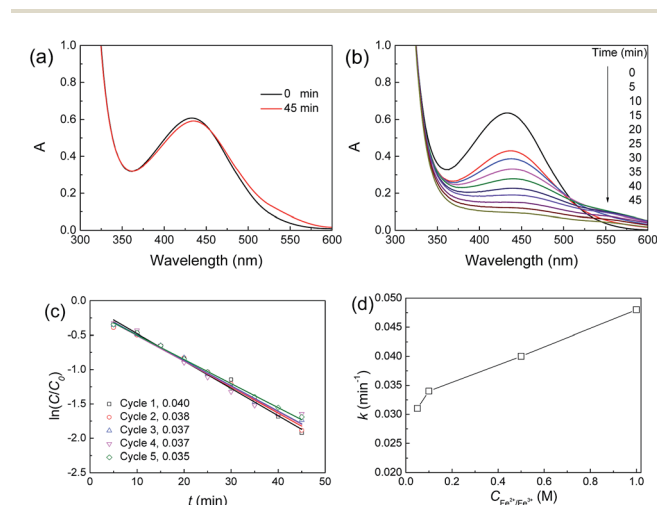
Acknowledgements

Fig. 8 (a and b) UV spectra of the XO solutions with H_2O_2 in the absence (a) or presence (b) of a JF/Fe$_3$O$_4$ nanocomposite hydrogel; (c) $\ln(C/C_0)$–t plots of the reaction catalyzed a JF/Fe$_3$O$_4$ nanocomposite hydrogel prepared at a Fe^{2+}/Fe^{3+} concentration of 0.5 M for five successive cycles; (d) k values of the reaction catalyzed a JF/Fe$_3$O$_4$ nanocomposite hydrogel prepared at different Fe^{2+}/Fe^{3+} concentrations.

References

1 D. Zhang, P. Sun, P. Li, A. Xue, X. Zhang, H. Zhang and X. Jin, *Biomaterials*, 2013, **34**, 10258–10266.

2 S. A. Meenach, C. G. Otu, K. W. Anderson and J. Z. Hilt, *Int. J. Pharm.*, 2012, **427**, 177–184.

3 F. Lu, H. Li, M. Sun, L. Fan, H. Qiu, X. Li and C. Luo, *Anal. Chim. Acta*, 2012, **718**, 84–91.

4 T. Liu, X. Zhang, B. Li, J. Ding, Y. Liu, G. Li, X. Meng, Q. Cai and J. Zhang, *RSC Adv.*, 2014, **4**, 50765–50770.

5 X. Zheng, D. Wu, T. Su, S. Bao, C. Liao and Q. Wang, *ACS Appl. Mater. Interfaces*, 2014, **6**, 19840–19849.

6 W. Wang, Y. Liu, T. Li and M. Zhou, *Chem. Eng. J.*, 2014, **242**, 1–9.

7 M. Zhu and G. Diao, *J. Phys. Chem. C*, 2011, **115**, 18923–18934.

8 V. K. Tripathi and R. Nagarajan, *J. Am. Ceram. Soc.*, 2016, **99**, 814–818.

9 P.-Y. Lee, H.-S. Teng and C.-S. Yeh, *Nanoscale*, 2013, **5**, 7558–7563.

10 M. Biswal, K. Bhardwaj, P. K. Singh, P. Singh, P. Yadav, A. Prabhune, C. Rode and S. Ogale, *RSC Adv.*, 2013, **3**, 2288–2295.

11 J. I. Kim, B. S. Lee, C. Chun, J.-K. Cho, S.-Y. Kim and S.-C. Song, *Biomaterials*, 2012, **33**, 2251–2259.

12 Y. Zhou, S. Fu, L. Zhang, H. Zhan and M. V. Levit, *Carbohydr. Polym.*, 2014, **101**, 75–82.

13 Y.-M. Liu, W. Wang, W.-C. Zheng, X.-J. Ju, R. Xie, D. Zerrouki, N.-N. Deng and L.-Y. Chu, *ACS Appl. Mater. Interfaces*, 2013, **5**, 7219–7226.

14 G. Magnacca, A. Allera, E. Montoneri, L. Celi, D. E. Benito, L. G. Gagliardi, M. C. Gonzalez, D. O. Mártire and L. Carlos, *ACS Sustainable Chem. Eng.*, 2014, **2**, 1518–1524.

15 S. Shin, H. Yoon and J. Jang, *Catal. Commun.*, 2008, **10**, 178–182.

16 S. Shylesh, V. Schuenemann and W. R. Thiel, *Angew. Chem.*, 2010, **49**, 3428–3459.

17 M. M. Moghaddam, B. Pieber, T. Glasnov and C. O. Kappe, *ChemSusChem*, 2014, **7**, 3122–3131.

18 Y. Moliner-Martinez, Y. Vitta, H. Prima-Garcia, R. A. Gonzalez-Fuenzalida, A. Ribera, P. Campins-Falco and E. Coronado, *Anal. Bioanal. Chem.*, 2014, **406**, 2211–2215.

19 J.-S. Chen, Y.-M. Zhang and X.-W. Lou, *ACS Appl. Mater. Interfaces*, 2011, **3**, 3276–3279.

20 F. Wang, X. Zhang, L. Shao, Z. Cui and T. Nie, *RSC Adv.*, 2015, **5**, 22188–22198.

21 G. Zou, K. Xiong, C. Jiang, H. Li, Y. Wang, S. Zhang and Y. Qian, *Nanotechnology*, 2005, **16**, 1584–1588.

22 H. Woo, K. Lee and K. H. Park, *ChemCatChem*, 2014, **6**, 1635–1640.

23 X. Xue, K. Hanna, C. Despas, F. Wu and N. Deng, *J. Mol. Catal. A: Chem.*, 2009, **311**, 29–35.

24 Z.-S. Wu, S. Yang, Y. Sun, K. Parvez, X. Feng and K. Muellen, *J. Am. Chem. Soc.*, 2012, **134**, 9082–9085.

25 T.-Y. Liu, S.-H. Hu, T.-Y. Liu, D.-M. Liu and S.-Y. Chen, *Langmuir*, 2006, **22**, 5974–5978.

26 L. Yu, B. J. Scherlag, K. Dormer, K. T. Nguyen, C. Pope, K.-M. Fung and S. S. Po, *Circulation*, 2010, **122**, 2653–2659.

27 P. Das, S. Yuran, J. Yan, P. S. Lee and M. Reches, *Chem. Commun.*, 2015, **51**, 5432–5435.

28 Y. Gao, Z. Wei, F. Li, Z. M. Yang, Y. M. Chen, M. Zrinyi and Y. Osada, *Green Chem.*, 2014, **16**, 1255–1261.

29 C.-H. Zhu, Y. Lu, J.-F. Chen and S.-H. Yu, *Small*, 2014, **10**, 2796–2800.

30 Y. Gao, C. Hu, W. J. Zheng, S. Yang, F. Li, S. D. Sun, M. Zrinyi, Y. Osada, Z. M. Yang and Y. M. Chen, *ChemPhysChem*, 2016, **17**, 1–10.

31 Z. Li, Z. Zheng, Y. Yang, G. Fang, J. Yao, Z. Shao and X. Chen, *ACS Sustainable Chem. Eng.*, 2016, **4**, 1500–1506.

32 G. R. Mahdavinia, S. Mousanezhad, H. Hosseinzadeh, F. Darvishi and M. Sabzi, *Carbohydr. Polym.*, 2016, **147**, 379–391.

33 Z. Yang and Z. Niu, *Chem. Commun.*, 2002, 1972–1973.

34 L. Ji, Z. Wang, Z. Li and J. Liang, *Mater. Lett.*, 2008, **62**, 1979–1982.

35 J. S. Im, B. C. Bai, S. J. In and Y.-S. Lee, *J. Colloid Interface Sci.*, 2010, **346**, 216–221.

36 B. F. Lin, K. A. Megley, N. Viswanathan, D. V. Krogstad, L. B. Drews, M. J. Kade, Y. Qian and M. V. Tirrell, *J. Mater. Chem.*, 2012, **22**, 19447–19454.

37 Q. Mao, S. Shi and H. Wang, *ACS Sustainable Chem. Eng.*, 2015, **3**, 1915–1924.

38 R. H. White and L. P. Hager, *Biochemistry*, 1977, **16**, 4944–4948.

39 T. Nagai, T. Ogawa, T. Nakamura, T. Ito, H. Nakagawa, K. Fujiki, M. Nakao and T. Yano, *J. Sci. Food Agric.*, 1999, **79**, 855–858.

40 J. Zhu, X. Wang, C. He and H. Wang, *J. Mech. Behav. Biomed. Mater.*, 2012, **6**, 63–73.

41 X. Wang, H. Wang and H. R. Brown, *Soft Matter*, 2011, **7**, 211–219.

42 Y.-N. Chen and H. Wang, *J. Colloid Interface Sci.*, 2015, **454**, 14–19.

43 Y.-X. Ma, Y.-F. Li, G.-H. Zhao, L.-Q. Yang, J.-Z. Wang, X. Shan and X. Yan, *Carbon*, 2012, **50**, 2976–2986.

44 C.-J. Jia, L.-D. Sun, F. Luo, X.-D. Han, L. J. Heyderman, Z.-G. Yan, C.-H. Yan, K. Zheng, Z. Zhang, M. Takano, N. Hayashi, M. Eltschka, M. Klaui, U. Rudiger, T. Kasama, L. Cervera-Gontard, R. E. Dunin-Borkowski, G. Tzvetkov and J. Raabe, *J. Am. Chem. Soc.*, 2008, **130**, 16968–16977.

45 G. Sun, B. Dong, M. Cao, B. Wei and C. Hu, *Chem. Mater.*, 2011, **23**, 1587–1593.

46 Y. Deng, D. Qi, C. Deng, X. Zhang and D. Zhao, *J. Am. Chem. Soc.*, 2008, **130**, 28–29.

47 X. Yang, X. Zhang, Y. Ma, Y. Huang, Y. Wang and Y. Chen, *J. Mater. Chem.*, 2009, **19**, 2710–2714.

48 J. Zhang, S. Xu and E. Kumacheva, *J. Am. Chem. Soc.*, 2004, **126**, 7908–7914.

49 M. Wang, N. Wang, H. Tang, M. Cao, Y. She and L. Zhu, *Catal. Sci. Technol.*, 2012, **2**, 187–194.

50 V. Iliev, D. Tomova, L. Bilyarska and L. Petrov, *Catal. Commun.*, 2004, **5**, 759–763.

51 D. Ayodhya, V. Maragoni, S. K. Amrutham, G. M. Kotu and V. Guttena, *IOSR J. Appl. Chem.*, 2013, **6**, 1–9.